XLVI CILAMCE
VITÓRIA - ES - BRAZIL - 2025
XLVI IBERO-LATIN AMERICAN CONGRESS ON COMPUTATIONAL METHODS IN ENGENEERING

Boundary Element Analysis of Fretting in Anisotropic Materials Under Centrifugal Loads

E. L. Albuquerque[1], L. S. Campos[2], W. R. Niz[1], L. B. Silva[1], T. Doca[1], F. M. Loyola[1]

[1]*Department of Mechanical Engineering, University of Brasilia*
Asa Norte, Brasília, 70910-900, DF, Brasil
eder@unb.br, weslei.niz@aluno.unb.br, bernardo.leonardo@aluno.unb.br,doca@unb.br, f.loyola91@gmail.com
[2]*Department of Mechanical Engineering, Federal University of Espirito Santo*
lucas.s.campos@ufes.br

Abstract. This work presents a boundary element method (BEM) to analyze frictional contact problems, with a focus on the fretting behavior in anisotropic materials subjected to centrifugal forces. A two-dimensional elastic BEM framework is developed, incorporating displacement constraints and force equilibrium to model the mechanical interaction between contacting bodies. The contact problem is inherently non-linear, as the initial contact area is unknown and evolves throughout the loading process. To account for centrifugal body forces, domain integrals are exactly converted into equivalent boundary integrals using the radial integration method. The proposed formulation is applied to a representative aeronautical application that involves contact between an anisotropic single-crystal metallic blade and an isotropic metallic rotor. The numerical results are compared with those obtained using the finite element method (FEM) to validate the precision and efficiency of the approach.

Keywords: Boundary element method, contact mechanics, fretting, anisotropic materials, centrifugal loads.

1 Introduction

In modern gas turbine engines, particularly those used in aerospace propulsion, turbine blades are subjected to severe mechanical and thermal stresses. These blades are typically attached to the turbine disc through dovetail joints, a mechanical interlocking configuration designed to withstand high centrifugal loads during operation [1]. However, cyclic loading conditions, resulting from engine start-up, normal operation, and shutdown, induce relative micro-movements at the contact interface between the blade root and the disc [2]. This repetitive microslip, in the presence of high contact pressures, causes the phenomenon of fretting [3].

Fretting fatigue is a degradation mechanism that results from the combination of fretting-induced damage and cyclic fatigue loading [4]. In dovetail joints, partial slip conditions commonly occur, where one portion of the contact interface adheres while another slips [5]. This results in highly localized stress concentrations, particularly in the transition between the stick and slip zones [6–8]. These stress concentrations significantly increase the likelihood of crack initiation and subsequent propagation under service loads, and can lead to premature failure of turbine components.

The severity of fretting fatigue in turbine blade attachments is further compounded by the material system in use. Single-crystal nickel (Ni)-based superalloys are widely used for the manufacturing of turbine blades due to their exceptional mechanical properties at elevated temperatures, including high creep resistance, oxidation resistance, and fatigue resistance [9–11]. However, these materials are inherently anisotropic, with mechanical responses strongly dependent on crystallographic orientation relative to the loading direction [12]. This anisotropy adds complexity to the analysis and prediction of fretting fatigue behavior, as the orientation of the crystal structure can influence both the initiation site and the path of crack propagation [11, 13].

Moreover, the interaction between single-crystal blades and polycrystalline discs at the dovetail joint introduces further challenges in modeling and life prediction. The mismatch in elastic and plastic properties across the interface can exacerbate local stress and strain fields, particularly under the multiaxial and non-proportional loading conditions characteristic of fretting [13]. Understanding these effects is essential for the development of reliable predictive models and the design of mitigation strategies aimed at improving the fatigue life of critical turbine components.

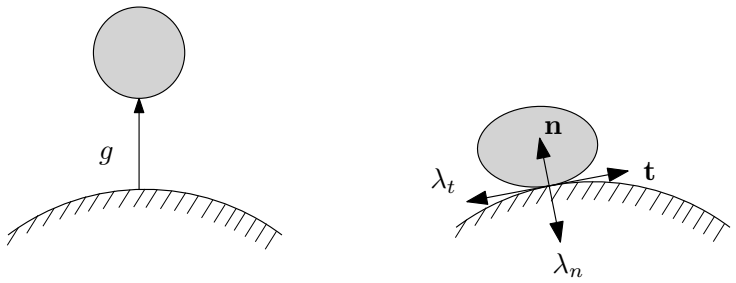


Figure 1. Bodies separated by an initial gap (left) and establishment of a contact condition (right).

In this context, numerical modeling plays a fundamental role in understanding the complex interaction between contact mechanics, material anisotropy, and multiaxial loading conditions. In particular, the Boundary Element Method (BEM) emerges as a powerful computational approach, capable of accurately capturing stress concentrations and contact behavior with a reduced computational cost compared to traditional methods. In this study, the boundary element method (BEM) is used to simulate the contact behavior and the evolution of the stress field associated with fretting fatigue in dovetail joints.

2 Contact formulation

A classical depiction of a contact process is given in Fig. 1. It encompasses two basic stages: 1) the evaluation of the normal gap, g, between the contact surfaces; and 2) the calculation of the contact pressure, λ_n, whenever the normal gap is closed.

This relationship is often denoted as the Kuhn-Karush-Tucker condition.

$$\begin{aligned} g &\geq 0, \\ \lambda_n &\leq 0, \\ \lambda_n g &= 0. \end{aligned} \tag{1}$$

Moreover, the contact conditions can be thought as constraints that must be satisfied for each node-pair within the contact zone. Therefore, they can be defined into three states:

- **Separated** is when both nodes are within a positive and nonzero distance from each other.
- **Stick** bodies are in contact while not showing tangential motion.
- **Slip** bodies are in contact and without restriction in the tangential direction.

Table 1 lists the relationships that represent the three modes of contact previously stated, where t_n and t_t are the normal and tangential tractions, and u_n and u_t are the normal and tangential displacements (expressed in local coordinates), respectively. It is important to note that the state of the node pairs is continuously updated within the

Table 1. Set of traction/displacement relations for the contact conditions.

Separated	**Stick**	**Slip**
$t_t^a - t_t^b = 0$	$t_t^a - t_t^b = 0$	$t_t^a - t_t^b = 0$
$t_n^a - t_n^b = 0$	$t_n^a - t_n^b = 0$	$t_n^a - t_n^b = 0$
$t_t^a = 0$	$u_t^a - u_t^b = 0$	$t_t^a \pm \mu t_n^a = 0$
$t_n^a = 0$	$u_n^a - u_n^b = g^{ab}$	$u_n^a - u_n^b = g^{ab}$

iterative procedure.

The proposed formulation addresses frictional contact in a two-dimensional setting. The solids are regarded as homogeneous isotropic linear elastic bodies. For example, let us consider the bodies A and B so that their deformations can be described by two coupled integral equations, one for each body, as follows.

$$c_{ij}^A u_j^A + \sum_{n=1}^{N_A} H_{ij}^A u_j^A = \sum_{n=1}^{NA} G_{ij}^A t_j^A \tag{2}$$

$$c_{ij}^B u_j^B + \sum_{n=1}^{N_B} H_{ij}^B u_j^B = \sum_{n=1}^{NB} G_{ij}^B t_j^B \tag{3}$$

where N_A and N_B are the number of collocation points of bodies A and B, respectively. Therefore, two sets of linear equations are obtained and their matrix form can be written such that

$$[H]^{\gamma}\{u\}^{\gamma} = [G]^{\gamma}\{t\}^{\gamma}\ ,\ \gamma = A, B \tag{4}$$

As noted in [14, 15], for linear problems, once this system of equations has been solved, the final solution for displacements and tractions everywhere on the boundaries can be obtained. This is not the case for this study, as we are dealing with a nonlinear problem. This nonlinearity comes from the fact that the contact region is not known *a priori* and must be determined as part of the solution. In order to overcome this, the same approach as used in [16–18] is employed here. It consists of an iterative method known as the generalized Newton method.

3 Results

In order to access the accuracy of the code, a numerical example is analyzed here. It consists of a dovetail joint of an aeronautic turbine in constant rotation. The disc and the blade are of the same single-crystal material. The input used in the program is as follows, the material properties and some dimensions are displayed in the table 2. The geometries of the model are as shown in Figs. 2 and 3. In figure 2 presents a 2D plot of the dovetail joint geometry of the disc and blade. It is intended to conceptually illustrate the components and their interface without including specific dimensions or applied boundary conditions. Its primary purpose is to provide a clear, unencumbered view of the joint's profile relevant to the contact region.

Table 2. Dimensions and material properties.

Property	**Symbol**	**Value**
Internal Radius	R	4.5 mm
External Radius	R	5 mm
Blades Length	w	120 mm
Disks Height	h	6.5 mm
Young's Modulus	E	73.4 GPa
Shear Modulus	G	57.6 GPa
Poisson's ratio	ν	0.44
Friction coefficient	f	0.3
Centrifugal Force	P	100 N

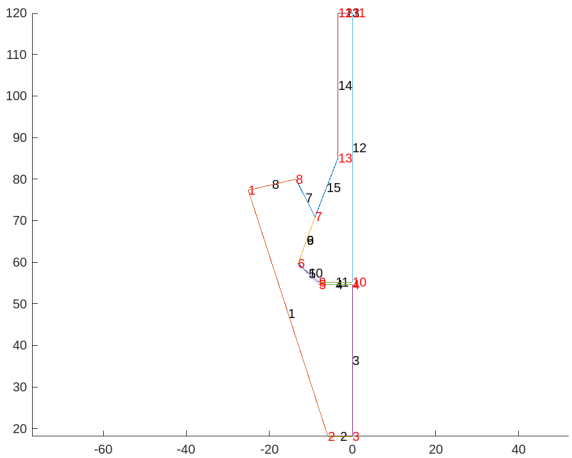


Figure 2. Dovetail BEM Setup

Figure 3 shows the boundary element mesh and boundary conditions of the disc and blade dovetail joint.

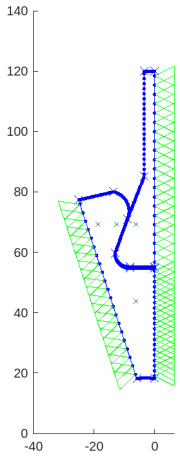


Figure 3. Dovetail BEM

Figure 4 shows the deformed mesh. The deformation is only due to the centrifugal load. As expected, the blade is pulled in the radial direction, and the contact region between the blade and the rotor suffers sliding of the surfaces.

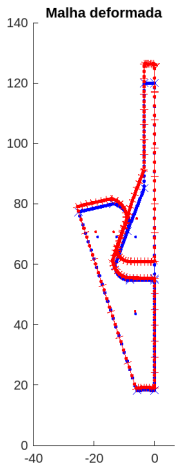


Figure 4. Tangential Displacement and Deformed Mesh

Figure 5 shows the tangential displacement within the contact zone of the blade. It can be seen that there is a sharp variation in displacements near the ends of the contact zone. This region coincides with the region where the variation in stress is also sharp. It is important to remember that the reference system is local, i.e., normal tangent $n - t$ instead of $x - y$. So, the positive values of the tangent displacement are those in the counter clockwise direction. This explains why the tangent displacements are negative.

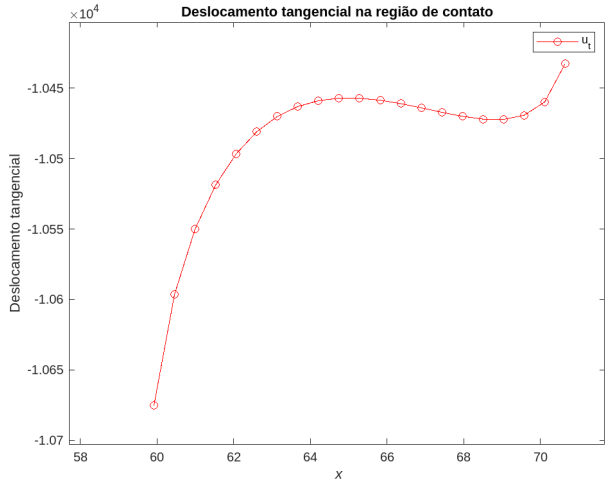


Figure 5. Tangential Displacement in the Contact Region

Figure 6 shows the magnitude of the normal displacement compared to the tangential displacements. Regions of high shear stress are typically found where tangential displacement gradients are steep, or at the ends of the contact zone where slip transit to separation. This correlation directly supports the understanding that localized shear stresses drive surface damage and crack initiation in fretting.

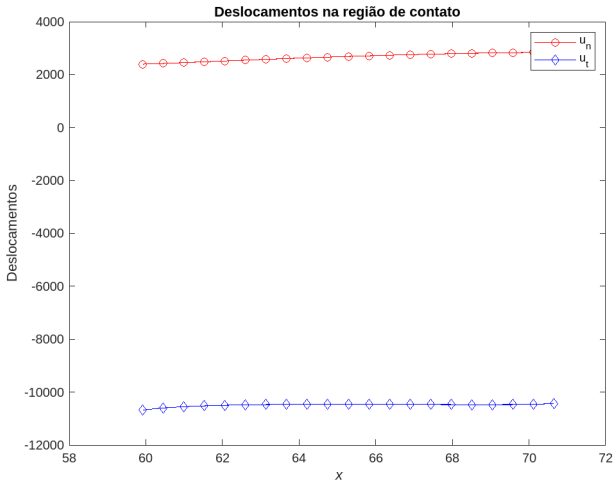


Figure 6. Displacements and Shear Stress

Figure 7 shows the stress magnitudes within the contact region. Tangent magnitudes are divided by the friction coefficient. As can be seen, both curves are coincident, indicating that the entire contact is in the slip-mode. The profile of these stresses along the contact interface allows for the identification of the peak stress locations. Fretting fatigue is driven by highly localized stress concentrations. The peaks and troughs observed in this graph correspond to areas of high stress concentration, which, in fretting, are typically found at the edges of the contact patch or at the stick-slip transition zones.

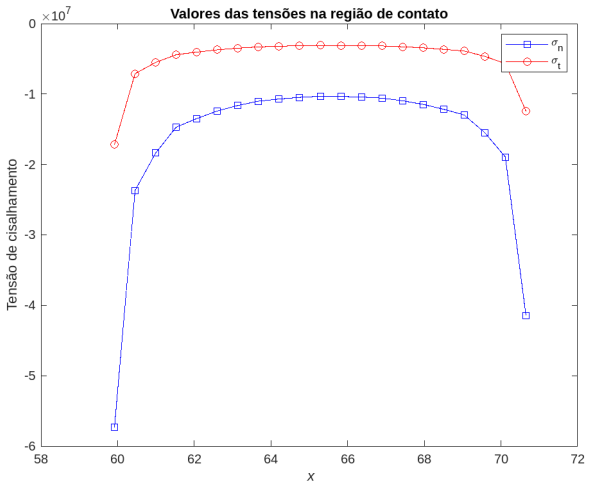


Figure 7. Stress Values in the Contact Region

Figure 8 presents the magnitude or absolute values of stresses, providing a scalar measure of the overall stress state within the contact region. The presentation of both normal stress and tangential stress divided by the friction coefficient provides a consistent view of the stress state.

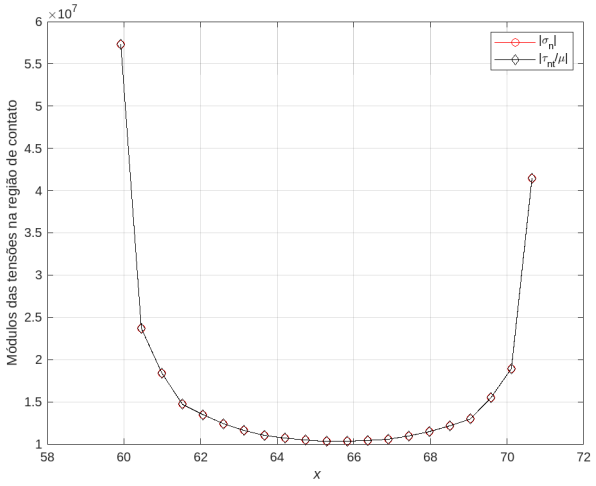


Figure 8. Stress Moduli in the Contact Region

4 Conclusions

This study presented a two-dimensional Boundary Element Method (BEM) formulation tailored for analyzing frictional contact problems under the influence of centrifugal forces, with a particular emphasis on fretting phenomena in anisotropic materials. The implementation effectively incorporated displacement compatibility and traction equilibrium to simulate the nonlinear nature of contact behavior, including the evolution of stick-slip regimes. The proposed BEM framework successfully addressed the challenges posed by anisotropy and body forces through an exact boundary-only representation, enabled by the radial integration method. The numerical results demonstrated the ability of the method to capture localized stress concentrations and tangential displacements along the contact interface, which are critical indicators of fretting-induced damage.

The stress and displacement profiles obtained in the contact zone are consistent with known fretting fatigue mechanisms, especially in regions near contact transitions, where high shear stress and relative motion were observed. The results also confirmed the robustness and computational efficiency of the BEM approach compared to traditional finite element analyzes, highlighting its suitability for parametric studies and fatigue life predictions in aeronautical applications. Future work may extend the current formulation to incorporate plasticity, temperature-

dependent material behavior, or crack propagation modeling to further enhance predictive capabilities in fretting fatigue assessments.

Acknowledgements. The authors appreciate the financial support provided by the Brazilian National Council for Scientific and Technological Development (CNPq), the Foundation for the Support of Research in the Federal District (FAP-DF) and the Brazilian Federal Agency for the Support and Evaluation of Graduate Education (CAPES).

Authorship statement. The authors hereby confirm that they are the sole liable persons responsible for the authorship of this work, and that all material that has been included herein as part of the present paper is either the property (and authorship) of the authors or has the permission of the owners to be included here.

References

[1] T. d. O. Vale, G. d. C. Villar, and J. C. Menezes. Methodology for structural integrity analysis of gas turbine blades. *Journal of Aerospace Technology and Management*, vol. 4, n. 1, pp. 51–59, 2012.
[2] R. Nalla, J. Campbell, and R. Ritchie. Mixed-mode, high-cycle fatigue-crack growth thresholds in ti–6al–4v: Role of small cracks. *International Journal of Fatigue*, vol. 24, n. 10, pp. 1047–1062, 2002.
[3] M. Nesládek, M. Španiel, J. Kuželka, J. Jurenka, and K. Doubrava. A fretting damage correction factor applicable to the mcdiarmid criterion of plain high-cycle fatigue. *Fatigue & Fracture of Engineering Materials & Structures*, vol. 40, n. 1, pp. 27–44, 2017.
[4] D. Nowell, D. Dini, and D. Hills. Recent developments in the understanding of fretting fatigue. *Engineering Fracture Mechanics*, vol. 73, n. 2, pp. 207–222. Advanced Fracture Mechanincs for Life Safety Assessments, 2006.
[5] S. L. Sunde, B. Haugen, and F. Berto. Experimental and numerical fretting fatigue using a new test fixture. *International Journal of Fatigue*, vol. 143, pp. 106011, 2021.
[6] J. Pauw, de P. baets, W. De Waele, and R. Hojjati. Contact mechanics in fretting fatigue. *International Journal Sustainable Construction & Design*, vol. 3, pp. 199–206, 2012.
[7] D. Croccolo, M. De Agostinis, S. Fini, G. Olmi, F. Robusto, and C. Scapecchi. Fretting fatigue in mechanical joints: A literature review. *Lubricants*, vol. 10, n. 4, 2022.
[8] L. H. L. Martins, J. C. T. Ferro, J. L. A. Ferreira, J. A. Araújo, and L. Susmel. A notch methodology to estimate fretting fatigue strength. *Journal of the Brazilian Society of Mechanical Sciences and Engineering*, vol. 29, pp. 82–90, 2007.
[9] H. Dong, Y. Chen, D. Wu, H. Ma, Z. Feng, and R. Su. Unlocking the potential of trace cobalt in ni-based superalloys: A molecular dynamics study on dislocation behavior and high-temperature stability. *Materials & Design*, vol. 253, pp. 113905, 2025.
[10] T. Saito, M. Yuyama, and H. Murakami. Effect of cobalt presence on creep properties of ni-based single crystal superalloys at intermediate temperature. *Journal of Alloys and Compounds*, vol. 1022, pp. 179871, 2025.
[11] L. Zhang, L. Zhao, R. Jiang, and C. Bullough. Crystal plasticity finite-element modelling of cyclic deformation and crack initiation in a nickel-based single-crystal superalloy under low-cycle fatigue. *Fatigue & Fracture of Engineering Materials & Structures*, vol. 43, n. 8, pp. 1769–1783, 2020.
[12] A. Long, X. Liu, J. Cheng, J. Xiong, G. Feng, J. Guo, and R. Liu. Anisotropy in creep behavior of a directionally solidified ni-based superalloy at 980 °c and 1070 °c. *Materials*, vol. 18, n. 9, 2025.
[13] P. Rajeev and T. Farris. Numerical analysis of fretting contacts of dissimilar isotropic and anisotropic materials. *The Journal of Strain Analysis for Engineering Design*, vol. 37, n. 6, pp. 503–517, 2002.
[14] K. Man, M. Aliabadi, and D. Rooke. Bem frictional contact analysis: Load incremental technique. *Computers & Structures*, vol. 47, n. 6, pp. 893–905, 1993a.
[15] K. Man, M. Aliabadi, and D. Rooke. BEM frictional contact analysis: Modelling considerations. *Engineering Analysis with Boundary Elements*, vol. 11, n. 1, pp. 77–85, 1993b.
[16] B. M. Cavalcante, M. H. Shaterzadeh-Yazdi, P. Sollero, E. L. Albuquerque, and T. Doca. Analysis of a Cattaneo-Mindlin problem using the Boundary Element Method. *Trib. Int.*, vol. 108, pp. 194–201, 2017.
[17] L. Rodríguez-Tembleque and R. Abascal. A FEM–BEM fast methodology for 3d frictional contact problems. *Computers & Structures*, vol. 88, n. 15-16, pp. 924–937, 2010.
[18] L. Rodríguez-Tembleque, F. García-Sánchez, and A. Sáez. Crack-face frictional contact modelling in cracked piezoelectric materials. *Computational Mechanics*, vol. 64, n. 6, pp. 1655–1667, 2019.